ADVANCED FUNCTIONAL MATERIALS
www.afm-journal.de

Dual Support System Ensuring Porous Co–Al Hydroxide Nanosheets with Ultrahigh Rate Performance and High Energy Density for Supercapacitors

*Xiaoliang Wu, Lili Jiang, Conglai Long, Tong Wei, and Zhuangjun Fan**

Layered double hydroxides (LDHs) are promising supercapacitor electrode materials due to their high specific capacitances. However, their electrochemical performances such as rate performance and energy density at a high current density, are rather poor. Accordingly, a facile strategy is demonstrated for the synthesis of the integrated porous Co–Al hydroxide nanosheets (named as GSP-LDH) with dual support system using dodecyl sulfate anions and graphene sheets as structural and conductive supports, respectively. Owing to fast ion/electron transport, porous and integrated structure, the GSP-LDH electrode exhibits remarkably improved electrochemical characteristics such as high specific capacitance (1043 F g^{-1} at 1 A g^{-1}) and ultra-high rate performance capability (912 F g^{-1} at 20 A g^{-1}). Moreover, the assembled sandwiched graphene/porous carbon (SGC)//GSP-LDH asymmetric supercapacitor delivers a high energy density up to 20.4 Wh kg^{-1} at a very high power density of 9.3 kW kg^{-1}, higher than those of previously reported asymmetric supercapacitors. The strategy provides a facile and effective method to achieve high rate performance LDH based electrode materials for supercapacitors.

1. Introduction

Compared with other chemical energy storage devices, supercapacitors have attracted considerable attention in the field of energy storage owing to their fast charge–discharge rate, long cycle lifetime, and high power density.[1–6] However, it is imperative to improve energy density to meet future emerging markets including hybrid vehicles and personal electronics. Recent research efforts have focused on exploring the improvement of capacitance and cell voltage that are critical factors to determine energy storage performance of supercapacitors.[3,7]

Commonly, carbon-based electrical double layer capacitors have already attracted extensive research due to their cost-effective, large surface area/porosity, excellent electrical conductivity, and extraordinary cycling stability.[6] However, their relatively low capacitance, often less than 300 F g^{-1}, are unfavourable for further improvement of the energy density of supercapacitors. Generally speaking, pseudocapacitive metal oxides /hydroxides, such as RuO_2, Co_3O_4, MnO_2, $Ni(OH)_2$, $Co(OH)_2$ and their binary systems, possess high pseudocapacitances from reversible faradic reaction.[8–13] Recently, metallic layered double hydroxides (LDHs) have attracted increasing interest as promising electrode materials for supercapacitor due to their relatively low cost, high redox activity, and environmentally friendly nature.[14–18] Although LDHs have high capacitance up to 1000 F g^{-1}, the rate capability and durability are rather poor due to their intrinsic insulation nature, especially, the specific capacitance drops dramatically at a high current density more than 20 A g^{-1}. For example, hollow Ni–Co double hydroxide microsphere had a specific capacitance up to 2275 F g^{-1} at 1 A g^{-1}, whereas the capacitance only maintained 44% at 25 A g^{-1}.[19] The Ni–Co LDH electrode displayed a specific capacitance of 2682 F g^{-1} at 3 A g^{-1}, whereas the capacitance only maintained 63% at 20 A g^{-1}.[15] Accordingly, achieving high energy density at high power density requires electrode materials with fast redox reaction and high electron-transfer rates. Recently, considerable interest has been focused on the design of nanostructured LDH materials with high surface area and porous structure, and the incorporation of high conductive nanocarbon (carbon nanotube, graphene) into the LDH composites.[16,20,21] Apart from the kinetics issue, structural stability of the electrode is also responsible for the enhanced rate performance and cycling stability due to the structure collapse of active materials, and reagglomeration into large grains during charge–discharge at high current densities. More importantly, to realize the full potential of the electrode materials, the tailored electrode structure should be taken full account of geometries, pore size and distribution, conductivity, and integral structure stability.[6]

In this work, the integrated porous Co–Al hydroxide nanosheets (GSP-LDH) with dual support system using dodecyl sulfate anions and graphene sheets as structural and conductive supports, respectively, were synthesized through anion intercalation, alkali etching, and electrostatic assembly of Co–Al LDH precursor, as shown in **Figure 1**a. The dodecyl sulfate anions are intercalated into the interlayer gallery of LDH to

Dr. X. L. Wu, Dr. L. L. Jiang, Dr. C. L. Long, Prof. T. Wei, Prof. Z. J. Fan
Key Laboratory of Superlight Materials and Surface Technology
Ministry of Education, College of Materials Science and Chemical Engineering
Harbin Engineering University
Harbin 150001, P. R. China
E-mail: fanzhj666@163.com

DOI: 10.1002/adfm.201404142

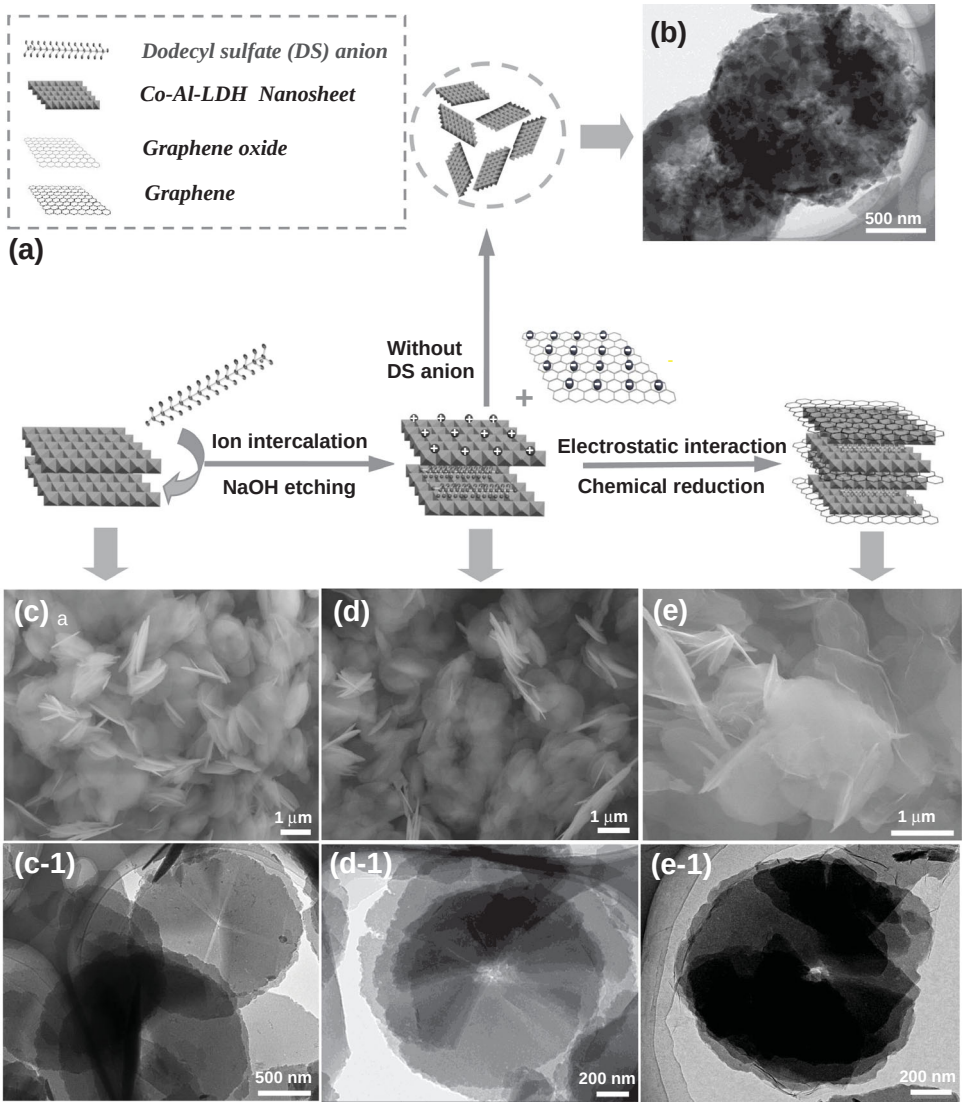

Figure 1. a) Schematic of the formation and structure of GSP-LDH composite. b) SEM and TEM images of P-LDH, c,c-1) LDH, d,d-1) SP-LDH, and e,e-1) GSP-LDH.

compensate for the loss of Al^{3+} during the partial removal of Al, resulting in the charge balance[22] and the enhanced interlayer spacing, as well as maintaining structure stability. After that, graphene and anion-intercalated LDH are assembled through the electrostatic interaction between graphene oxide (GO) and LDH,[23] and consequent chemical reduction. Benefiting from fast ion transport, high conductivity, porous and integrated structure, the obtained porous LDH with dual support system delivers a high specific capacitance of 1043 F g^{-1} at a current density of 1 A g^{-1} and excellent rate performance (912 F g^{-1} at 20 A g^{-1}), as well as excellent cycling stability with 88% of its initial capacitance retention after 3000 cycles. Moreover, the assembled asymmetric supercapacitor sandwiched graphene/porous carbon (SGC)//GSP-LDH delivers an energy density of 41.2 Wh kg^{-1} (based on the total mass of the active material in both electrodes) at a power density of 185.4 W kg^{-1}, as well as good cycling performance with 84% of its initial capacitance retention after 2000 cycles. Even at a very high power density of 9.3 kW kg^{-1}, it still remains an energy density of 20.4 Wh kg^{-1}, higher than those of other previously reported asymmetric supercapacitors.[3,11]

2. Results and Discussion

The morphologies and microstructures of the as-prepared samples were shown in Figure 1b–e. Scanning electron microscopy (SEM) image shows that Co–Al LDH exhibits 2D sheet-like structure with a lateral size less than 2 μm (Figure 1c). Transmission electron microscopy (TEM) images further confirm that the nanosheets have multi-layer restacking structure with the thickness of less than 50 nm (Figure 1c-1 and Figure S1a,b, Supporting Information). More importantly, after NaOH etching of dodecyl sulfate anion-intercalated LDH (named as SP-LDH), the morphology of SP-LDH still remains its original structure (Figure 1d), and the color of SP-LDH

suspension changes from pink to sandybrown in 0.5 M NaOH solution (Figure S2b, Supporting Information). Compared with pure LDH, there are more mesopores on the surface of LDH after NaOH etching (Figure S1c,d, Supporting Information). It is evident that Co/Al atomic ratio of ca.4.5:1 based on energy-dispersive X-ray spectroscopy for LDH after NaOH etching is higher than that of the initial LDH (3:1), indicating the partial removal of Al from LDH. When SP-LDH was treated in 1 M NaOH, the color of SP-LDH suspension showed dark brown and the whole structure of SP-LDH was destroyed (Figure S2h,i, Supporting Information). Whereas, without the protection of LDH by dodecyl sulfate anions in 0.5 M NaOH, the color of alkali etched LDH (named as P-LDH) suspension was dark brown (Figure S2c, Supporting Information), and LDH sheets were broken into many small sheets (Figure 1b). Moreover, the dark-pink was clearly observed after mixing negative charged GO (zeta potential: –37 mV) and positive charged SP-LDH (+40 mV) due to the electrostatic interaction (Figure S2e, Supporting Information). Therefore, graphene/SP-LDH hybrid material with layered structure are engineered by electrostatic interaction and subsequent chemical reduction using hydrazine hydrate (Figure 1e). High-resolution TEM (HRTEM) image further confirms face-to-face assembling between graphene sheet and SP-LDH sheet (**Figure 2**a and Figure S1e, Supporting Information). Moreover, X-ray elemental mappings confirm that atoms Co, Al, C, and O are homogeneously distributed throughout the GSP-LDH hybrid material (Figure S3, Supporting Information). Therefore, SP-LDH strongly coupled with conductive graphene is beneficial for the enhanced conductivity of pseudocapacitive materials.[24]

It is worth mentioning that there are two kinds of mesopores with the sizes of 2–5 nm (Figure 2b) and 5–20 nm (Figure 2a) in the surface of GSP-LDH. Furthermore, the pore structure and specific surface area of GSP-LDH were investigated by the nitrogen adsorption-desorption isotherms (Figure S1f, Supporting Information). The surface area of GSP-LDH (35.68 $m^2 g^{-1}$) is higher than those of pure LDH (25.51 $m^2 g^{-1}$), P-LDH (32.72 $m^2 g^{-1}$), and SP-LDH (34.48 $m^2 g^{-1}$), meaning the existence of porous structure after NaOH etching. The type IV isotherm of GSP-LDH exhibits a small hysteresis between the adsorption and desorption branches and steep rise in adsorption at 0.2–0.8 P/P_o, indicating the existence of mesopores with the pore size distribution of 2–20 nm calculated by the density functional theory (DFT) method, which is in good agreement with TEM observations. Additionally, the pore sizes about 1–2 nm are increased to 2–4 nm when P-LDH is incorporated with dodecyl sulfate anions, meaning that anions are effectively intercalated into LDH (Figure 2c).

X-ray powder diffraction (XRD) pattern of LDH is consistent with the standard compound $Co_6Al_2CO_3(OH)_{16}\cdot H_2O$ (JCPDF:51–0045) with the characteristic peaks of (003), (006), (012), and (015) planes (Figure 2d).[25,26] Additionally, P-LDH shows almost the same characteristic diffraction peaks as pure LDH, confirming that NaOH treatment will not cause phase changes. More interestingly, (003) diffraction peak of SP-LDH shifts to lower angle than that of LDH, suggesting the existence of dodecyl sulfate anions intercalated between the interlayer gallery of LDHs. Fourier transform infrared (FT-IR) spectra (Figure S4, Supporting Information) of GSP-LDH exhibits that the bands at 2918 and 2850 cm^{-1} are attributed

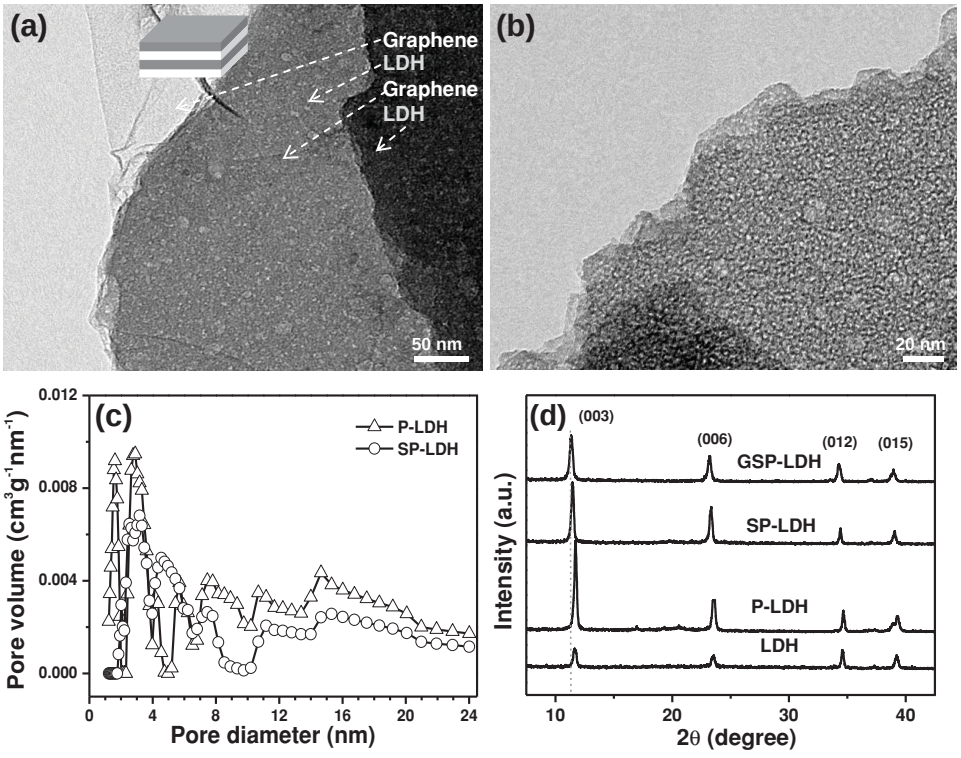

Figure 2. a,b) TEM images of GSP-LDH, exhibiting graphene-SPLDH-graphene closely stacking structure. c) Pore size distribution curves of P-LDH and SP-LDH. d) XRD patterns of LDH, P-LDH, SP-LDH, and GSP-LDH.

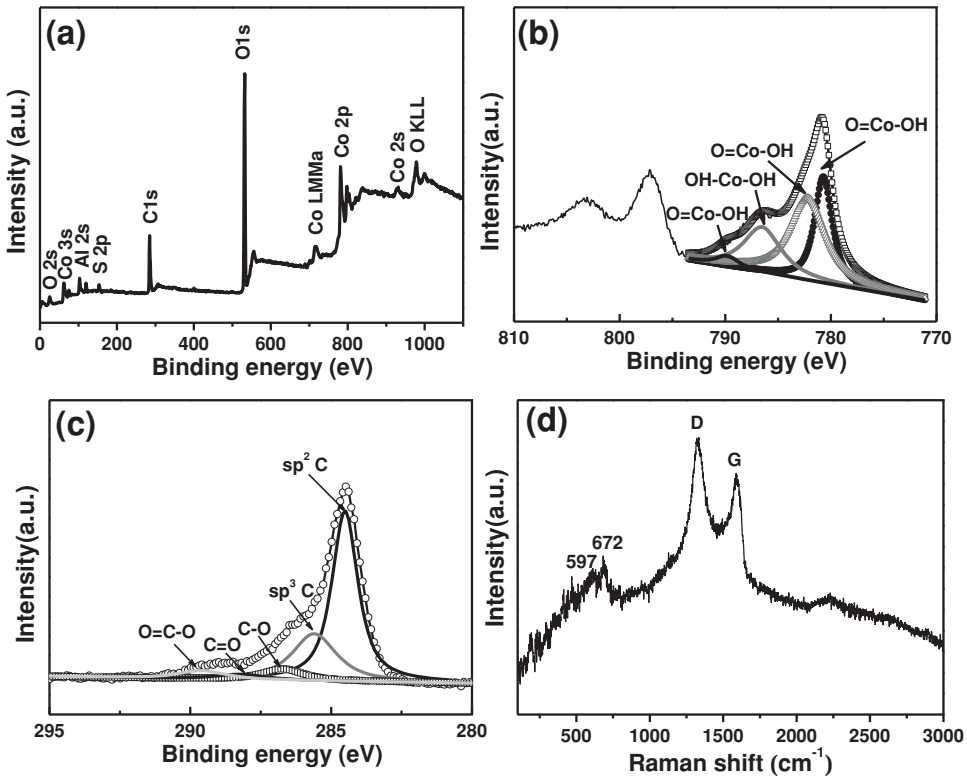

Figure 3. a) XPS spectrum of GSP-LDH, b) XPS high-resolution spectra of sample GSP-LDH Co 2*p*, c) XPS high-resolution spectra of sample GSP-LDH C1s. d) Raman spectrum of the GSP-LDH sample.

to $-CH_2$ stretching vibrations of alkyl chains of dodecyl sulfate, and bands in the range from 1300 to 900 cm^{-1} for the stretching mode of sulfate (OSO_3^-). Additionally, the valence change for GSP-LDH was investigated by X-ray photoelectron spectroscopy (XPS, **Figure 3**a). Notably, high-resolution Co_{2p} XPS spectrum of GSP-LDH reveals spin–orbit splitting into Co $2p_{1/2}$ and Co $2p_{3/2}$ components, and the Co $2p_{3/2}$ satellite line intensity is rather low (Figure 3b), suggesting the coexistence of Co^{2+} and Co^{3+} in LDH. Additionally, C 1s peak of GSP-LDH presents that five peaks centered at 284.5, 285.6, 286.7, 288.2 and 289.9 eV can be attributed to sp^2 C, sp^3 C, C–O, C=O, and O=C–O (Figure 3c),respectively, meaning partial removal of oxygen containing functional groups. Raman analysis (Figure 3d) exhibits that the intensity ratio (I_D/I_G) of reduced-GO (1.02) is higher than that of pure GO (0.86), suggesting the presence of unrepaired defects after the removal of partial oxygen moieties. In addition, two strong peaks located at 597 and 672 cm^{-1} are typically assigned to CoAl-LDH.[27]

Owing to unique structural and conductive supports, the GSP-LDH electrode is expected to possess excellent electrochemical properties at high charge-discharge rates for supercapacitors. The electrochemical properties of as-prepared samples measured in 6 M KOH electrolyte are shown in **Figure 4**. The CV curves of samples LDH, P-LDH, SP-LDH, and GSP-LDH exhibit a pair of redox peaks (Figure 4a), which are the typical faradic reaction of Co hydroxides in alkaline electrolyte.[28] The possible electrochemical reaction could be based on Equations (1),(2):

$$Co(OH)_2 + OH^- \leftrightarrow CoOOH + H_2O + e^- \quad (1)$$

$$CoOOH + OH^- \leftrightarrow CoO_2 + H_2O + e^- \quad (2)$$

In particular, the introduction of graphene sheets or dodecyl sulfate anions into the LDH can lead to a higher peak current compared to pure LDH, meaning a higher charge capacity. Moreover, the galvanostatic discharge curves for LDH, P-LDH, SP-LDH, and GSP-LDH at 1 A g^{-1} show typical pseudocapacitive characteristics (Figure 4b). The specific capacitance (C_s, F g^{-1}) can be calculated according to the following equation:

$$C_s = I\Delta t/(m\Delta V) \quad (3)$$

where I is the current density, Δt is the discharge time, m represents the mass of active material in the electrode, and ΔV is the electrochemical window. Accordingly, the specific capacitance of the GSP-LDH electrode is calculated to be 1043 F g^{-1} at 1 A g^{-1}(Figure 4c), higher than those of SP-LDH (927 F g^{-1}), P-LDH (849 F g^{-1}), and LDH (756 F g^{-1}) and other LDH-carbon hybrid materials.[23,29] Moreover, the capacitance retention ratios (C_{sp} at 20 A g^{-1}/C_{sp} at 1 A g^{-1}) of LDH, P-LDH, SP-LDH, and GSP-LDH are 44%, 63%, 78%, and 87% (Figure 4d), respectively. Therefore, the GSP-LDH electrode shows ultrahigh rate capability of 87%, much higher than those of previously reported LDH based materials (**Table 1**), such as Ni–Co LDH (44% from 1 A g^{-1} to 20 A g^{-1}),[19] Ni–Co–Al LDH (57% from 1 A g^{-1} to 30 A g^{-1}),[28] and Co–Al LDH/graphene (73% from 1 A g^{-1} to 10 A g^{-1}).[33]

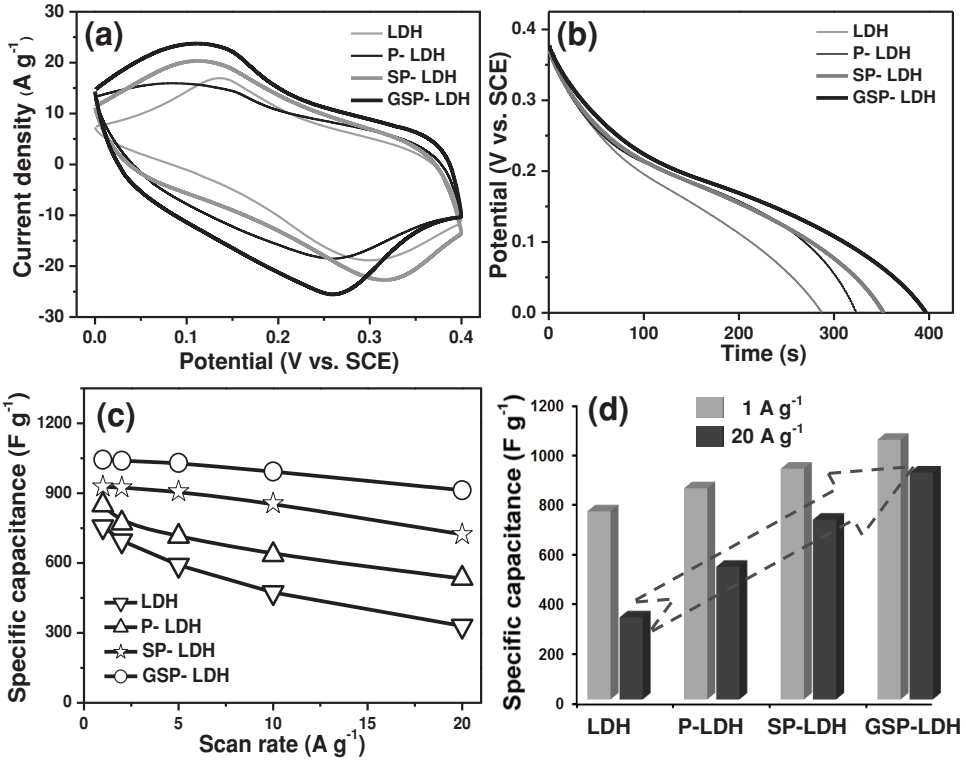

Figure 4. a) CV curves of LDH, P-LDH, SP-LDH and GSP-LDH at a scan rate of 20 mV s^{-1} in 6 M KOH electrolyte. b) Discharge curves of LDH, P-LDH, SP-LDH and GSP-LDH at a current density of 1 A g^{-1} in 6 M KOH aqueous electrolyte. c) Specific capacitances of LDH, P-LDH, SP-LDH, and GSP-LDH at different current densities. d) Specific capacitances of different electrode materials at 1 and 20 A g^{-1}.

To investigate the electrode kinetics, electrochemical impedance spectroscopy (EIS) measurements were performed as shown in Figure S5a, The ohmic resistance of the electrolyte and cell components (R (e)) of the GSP-LDH electrode is 0.37 Ω, which is smaller than those of LDH (0.74 Ω), P-LDH (0.56 Ω), and SP-LDH (0.44 Ω), meaning a much better ion diffusion property. Moreover, in the low frequency region, the GSP-LDH electrode exhibits a nearly vertical line, indicating high electron mobility. The impedance frequency behavior was further investigated by the complex model of the capacitance ($C(w)$). The normalized $C'(w)$ and $C''(w)$ as a function of frequency for the P-LDH and SP-LDH electrodes are presented in Figure S5 b,c. It can be obviously seen that the $C'(w)$ of the SP-LDH electrode deteriorates more slowly than that of the P-LDH electrode with the increase of frequency, which is attributed to fast ion diffusion and transport within the electrode. In addition, a time constant defined as $\tau_0 = 1/f_0$, which is known as a dielectric relaxation time characteristic of the whole system, is obtained from the maximum $C''(w)$ at frequency f_0. The τ_0 is 0.58 s for the SP-LDH electrode (based on Equations (5)–(7)), much lower than that of the P-LDH electrode (τ_0 = 0.84 s), demonstrating fast ion diffusion.

Table 1. Comparison of the rate capability of LDH based electrodes in the references.

Materials	Capacitance [F g^{-1}]	Rate capability [%]	Ref.
Ni-Co LDH	2275 (1 A g^{-1})	44% (25 A g^{-1})	[19]
Co–Al LDH	1075 (5 mA cm^{-2})	72% (50 mA cm^{-2})	[25]
Co–Al LDH/Pt	734 (1 A g^{-1})	61% (25 A g^{-1})	[26]
Ni-Co-Al-LDH	1289 (1 A g^{-1})	57% (30 A g^{-1})	[28]
Co–Al LDH/graphene	772 (1 A g^{-1})	80% (25 A g^{-1})	[29]
Ni–Co LDH	1000 (5 mv s^{-1})	69% (500 mv s^{-1})	[30]
$Co(OH)_2$	1116 (2 A g^{-1})	38% (10 A g^{-1})	[31]
Ni–Co–Al LDH/RGO/CNT	1188 (1 A g^{-1})	72% (10 A g^{-1})	[32]
Co–Al LDH/graphene	712 (1 A g^{-1})	73% (10 A g^{-1})	[33]
GSP-LDH	1043 (1 A g^{-1})	87% (20 A g^{-1})	This work

As known, long-term cycling stability is a critical parameter for evaluating the electrochemical performance of supercapacitors.[34] It can be clearly observed that the GSP-LDH electrode exhibits a capacitance retention ratio of 88% after 3000 cycles (Figure S5d, Supporting Information), higher than those of Co–Al LDH (76%), Ni–Co–Al LDH (82% after 2000 cycles),[26] and Co–Al LDH/graphene (81% after 2000 cycles),[33] demonstrating excellent long-term electrochemical stability. Therefore, the excellent electrochemical performances of the GSP-LDH electrode should be attributed to its unique structures. Firstly, the partial removal of Al from Co–Al LDH precursor generates more mesopores in favor of fast ion diffusion. Secondly, the intercalated anions can enhance the interlayer spacing and maintain the structure stability of LDH, resulting in good electrochemical stability. Finally, face-to-face assembly of graphene

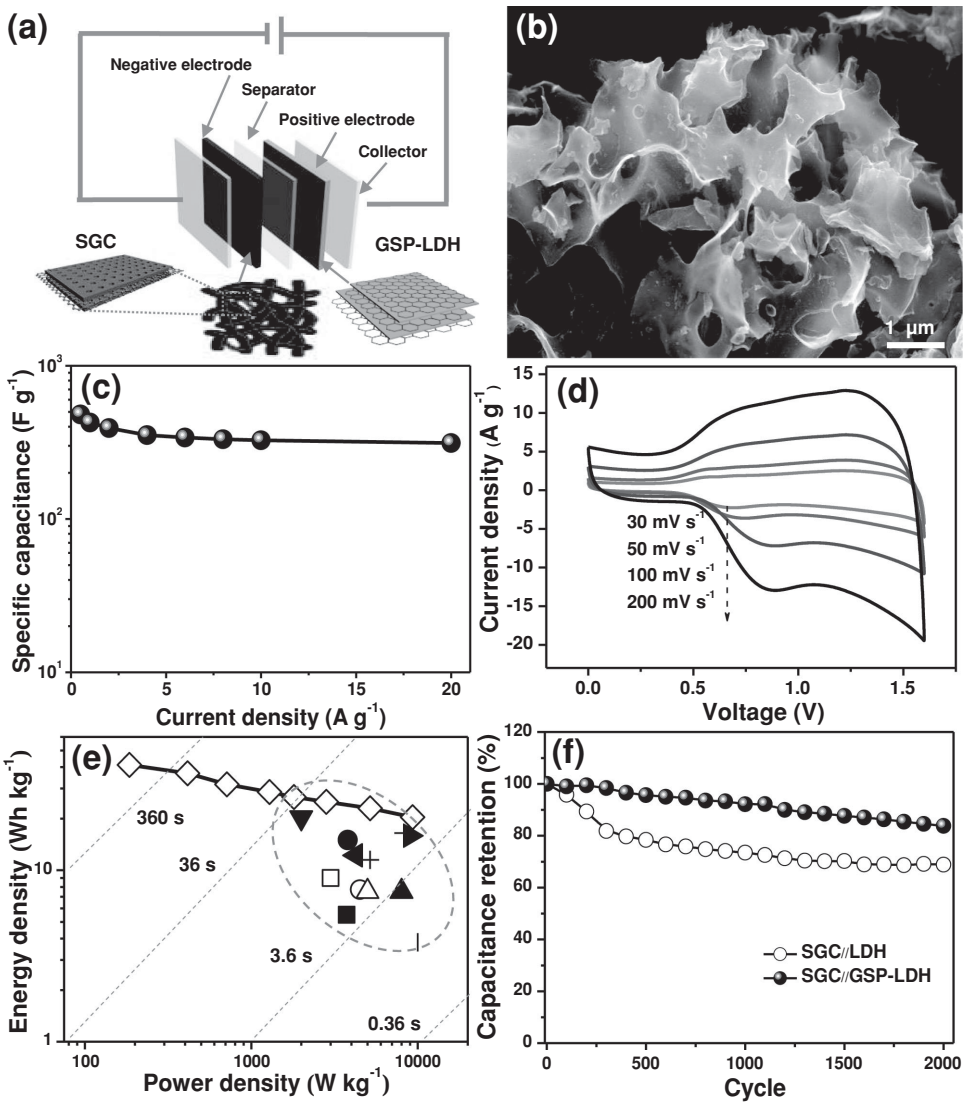

Figure 5. a) Schematic illustration of the fabricated asymmetric supercapacitor based on SGC as negative electrode and GSP-LDH as positive electrode. b) SEM image of SGC. c) Specific capacitances of the SGC electrode at different current densities. d) CV curves of SGC//GSP-LDH asymmetrical supercapacitor at different scan rates in 6 M KOH aqueous electrolyte. e) Ragone plot related to energy and power densities of the as-assembled SGC//GSP-LDH (☆),SGC// LDH asymmetric supercapacitor (◆) and other asymmetric supercapacitors previously reported in the literature, such as activated carbon//graphene/MnO_2 (★),[3] Co–Al LDH/GO//Co–Al LDH/GO (○),[13] Co–Al LDH/Pt// Co–Al LDH/Pt (◁) ,[28] VN//$Co(OH)_2$ (▶),[36] activated carbon//NiO/Ni (▲),[37] graphene// MnO_2/graphene (△),[38] graphene/MoO_3//graphene/MnO_2 (□),[39] V_2O_5/CNT//MnO_2/ activated carbon (■),[40] activated graphene//Co_3O_4/MnO_2 (▽),[41] activated carbon//$NaMnO_2$ (◀),[42] FeOOH//MnO_2 (●),[43] and AC//V_2O_5 (◇).[44] f) the long-term cycling performances of SGC//LDH and SGC//GSP-LDH asymmetric supercapacitors within a voltage window of 1.6 V at 100 mV s^{-1}.

and SP-LDH is beneficial for electron transport within the electrode.

Asymmetric supercapacitors (ASCs) have high energy densities due to the extension of the cell voltage window.[3,11] Recently, we had reported ASCs with a high energy density of 77.8 Wh kg^{-1} at a power density of 174.7 W kg^{-1} using porous graphene and graphene/$Ni(OH)_2$ as the negative and positive electrodes, respectively, however, it only remained 17.4 Wh kg^{-1} at a power density of 7.9 kW kg^{-1}.[11] Therefore, it is a great challenge to maintain high energy density at high power density. In this work, ASCs were assembled using sandwiched graphene/porous carbon (SGC) as negative electrode material and GSP-LDH as positive electrode material (**Figure 5**a). SGC was prepared by a facile one-step pyrolysis of the mixture of KOH and graphene oxide/polyaniline (PANI) precursor based on our previously work.[35] Due to its interconnected conducting network (Figure 5b), ultrahigh specific surface area (2927 cm^2 g^{-1}), and high nitrogen doping (6 at%), SGC exhibits high specific capacitance of 481 F g^{-1} at a current density of 0.5 A g^{-1}, and still maintains 313 F g^{-1} at 20 A g^{-1} (Figure 5c). Moreover, CV curves of as-assembled SGC//GSP-LDH asymmetric supercapacitor measured at the scan rates from 30 to 200 mV s^{-1} in 6 M KOH exhibit both pseudocapacitive and double-layer behaviors (Figure 5d). The energy and power densities of the SGC//GSP-LDH cell were shown in the Ragone plot (Figure 5e). Notably, the SGC//GSP-LDH asymmetric supercapacitor

shows an energy density of 41.2 Wh kg^{-1} at a power density of 185.4 W kg^{-1} (based on the total mass of the active material in both electrodes). Even at a high power density of 9.3 kW kg^{-1}, it still remains an energy density of 20.4 Wh kg^{-1}, higher than those of SGC//LDH (11.5 Wh kg^{-1} at 5.2 kW kg^{-1}) and other previously reported asymmetric supercapacitors, such as activated carbon//graphene/MnO_2 (16.5 Wh kg^{-1} at 8.2 kW kg^{-1}),[3] porous graphene//graphene/$Ni(OH)_2$ (17.4 Wh kg^{-1} at 7.9 kW kg^{-1}),[11] VN//$Co(OH)_2$ (15.9 Wh kg^{-1} at 9 kW kg^{-1}),[36] graphene//graphene/MnO_2 (7.0 Wh kg^{-1} at 5.0 kW kg^{-1}),[38] graphene/MoO_3//graphene/MnO_2 (9 Wh kg^{-1} at 3 kW kg^{1}),[39] activated carbon//$NaMnO_2$ (12.2 Wh kg^{-1} at 4.25 kW kg^{-1}),[42] FeOOH//MnO_2 (15 Wh kg^{-1} at 3.8 kW kg^{-1}),[43] and activated carbon//V_2O_5 (20.3 Wh kg^{-1} at 2 kW kg^{-1}).[44] Moreover, the long-term cycling performances of SGC//LDH and SGC//GSP-LDH asymmetric supercapacitors at 100 mV s^{-1} for 2000 cycles are shown in Figure 5f. Notably, the SGC//GSP-LDH asymmetric supercapacitor displays excellent cycling stability with about 84% of the initial capacitance retention, higher than those of SGC//LDH (69% after 2000 cycles) and previously reported ASCs, such as graphene//graphene/MnO_2 (79% after 1000 cycles),[38] activated carbon//$Ni(OH)_2$ (82% after 1000 cycles),[45] and activated carbon//$LiNi_{1/3}Co_{1/3}Mn_{1/3}O_2$ (80% after 1000 cycles).[46]

Accordingly, the SGC//GSP-LDH asymmetric supercapacitor delivers high energy density even at high power density, as well as excellent cycling stability, which are attributed to the enhanced electrochemical kinetics, good mechanical and structural stability, and fast charge transfer for the electrodes.

3. Conclusion

In summary, a facile synthetic route has been developed to directly assemble the integrated porous Co–Al hydroxide nanosheets with dual support system using dodecyl sulfate anions and graphene sheets as the structural and conductive support, respectively. Due to fast ion transport, high conductivity, porous and integrated structure,the as-obtained GSP-LDH shows a high specific capacitance, excellent rate performance, and excellent cycling stability. Moreover, the assembled SGC//GSP-LDH asymmetric supercapacitor delivers a high energy density up to 20.4 Wh kg^{-1} at a very high power density of 9.3 kW kg^{-1}, and excellent cycling stability. Therefore, the assembly design strategy would pave a simple and useful way to fabricate high-performance electrode materials for energy-storage devices such as supercapacitor, Li-ion batteries and fuel cell.

4. Experimental Section

Synthesis of LDH: In a typical procedure, 0.03 mol $Co(NO_3)_2{\cdot}6H_2O$, 0.01 mol $Al(NO_3)_3{\cdot}9H_2O$ and 0.1 mol $CO(NH_2)_2$ were dissolved in 200 mL distilled water. Then the above solution was transferred into a three-necked flask, and heated and refluxed at 90 °C for 8 h. Finally, the resulting product was filtered, washed with distilled water and ethanol several times, and freeze-dried.

Synthesis of Exfoliated LDH: 200 mg of the above obtained LDH was dispersed into 200 ml of formamide in a conical beaker, which was tightly capped after purging with nitrogen gas. Then, the mixture was agitated vigorously stirring for 2 days. Afterward, the mixture was further treated by centrifugation at 6000 rpm for 5 min and washed three times with distilled water. Finally, the resulting product was freeze-dried.

Synthesis of P-LDH: The above obtained exfoliated LDH (0.1 g) was added into 100 mL distilled water, and sonicated for 30 min. Then, 2.0 g NaOH was added into the above suspension and stirred for 12 h at room temperature. Finally, the resulting product was filtered, washed with distilled water and ethanol several times, and freeze-dried.

Synthesis of SP-LDH: The obtained exfoliated LDH (0.1 g) was added into 100 mL distilled water and sonicated for 30 min. Afterwards, 0.3842 g sodium dodecyl sulfate was added into above suspension and stirred for 10 min. Then, 2.0 g NaOH was added into the above suspension, and stirred for 12 h at room temperature. Finally, the resulting product was filtered, washed with distilled water and ethanol several times,and freeze-dried.

Synthesis of GSP-LDH Composite: GO was synthesized from natural graphite (Qingdao Graphite Company) by a modified Hummers method.[47] The above obtained SP-LDH (0.098 g) was added into 100 mL distilled water with a bit alcohol, and sonicated for 30 min. Afterwards, 20 mL of GO suspension (0.1 mg mL^{-1}) was added into the above suspension under vigorous stirring for 5 min. Then, the mixture solution was transferred into a one-necked flask, 350 μL of ammonia (32% in water) was added to keep the suspension under basic conditions. Subsequently, 100 μL of hydrazine hydrate (80% in water) were added, and the mixture solution was heated to 95 °C for 10 h. Finally, the resulting product was filtered, washed with distilled water and ethanol several times, and freeze-dried.

Material Characterizations: The crystallographic structure of the samples was determined by X-ray diffraction (XRD) equipped with Cu Kα radiation (λ = 0.15406 nm). X-ray photoelectron spectroscopy (XPS) was performed using a PHI5700ESCA spectrometer with a monochromated Al Kα radiation (hv=1486.6 eV), all of the data acquisition and processing were done on XPSPEAK software. The microstructures of the samples were investigated by field-emission scanning electron microscope (SEM, Camscan Mx2600FE) and transmission electron microscope (TEM, JEOL JEM2010). Fourier transform infrared (FT-IR) spectroscopy was carried out on a Perkin-Elmer Spectrum 100 spectrometer in a range of 500–4000 cm^{-1}. Raman spectra were conducted on a Jobin-Yvon HR800 spectrometer with 458 nm wavelength incident laser light. Pore structure of the samples were characterized by N_2 adsorption at 77 K using Barrett–Emmett–Teller (BET) calculations for the surface area. The pore size distribution was conducted on the adsorption branch of the isotherm using density functional theory (DFT) model.

Electrochemical Measurement: The fabrication of working electrodes were carried out as follows: Briefly, the active materials (75 wt%), carbon black (20 wt%), and polytetrafluoroethylene (5 wt%) were mixed and dispersed in ethanol to obtain a slurry, which was then coated onto the nickel foam current collectors (1 cm × 1 cm) with a spatula. Finally, the as-fabricated electrodes were dried at 80 °C for 12 h in a vacuum oven. The mass loading of the electrode materials was about 2 mg cm^{-2}. The asymmetric supercapacitor was built with a glassy fibrous separator and performed in a two-electrode cell in 6 M KOH aqueous electrolyte. The loading mass ratio of positive electrode material and negative electrode material was estimated from the equation as followed:

$$\frac{m_+}{m_-} = \frac{C_- \times V_-}{C_+ \times V_+} \tag{4}$$

where C is the specific capacitance (F g^{-1}), V is the potential range for the charge/discharge process (V) and m is the mass of the electroactive electrode (g). The electrochemical tests of the individual electrode were tested in a three-electrode cell. Ni foam coated with samples as the working electrode, platinum foil and saturated calomel electrode (SCE) as the counter and reference electrodes. The measurements were carried out in a 6 M KOH aqueous electrolyte at room temperature. All of the above electrochemical measurements were measured by a CHI 660C electrochemical workstation. The $C(w)$ is dependent on real part the cell capacitance $C'(w)$, the imaginary part $C''(w)$ related to the losses of energy dissipation and frequency, which is defined as follows: [48]

$$C = C'(w) - jC''(w) \quad (5)$$

$$C'(w) = \frac{-Z''(w)}{w|Z(w)|^2} \quad (6)$$

$$C''(w) = \frac{-Z'(w)}{w|Z(w)|^2} \quad (7)$$

where $Z'(w)$ and $Z''(w)$ are the respective real and imaginary parts of the complex impedance $Z(w)$. w is the angular frequency which is given by $w = 2\pi f$. The energy density (E) and power density (P) were calculated according to the following equations:

$$E = 0.5CV^2 \quad (8)$$

$$P = \frac{E}{\Delta t} \quad (8)$$

where Δt is indicating the discharge time (s).

Supporting Information

Supporting Information is available from the Wiley Online Library or from the author.

Acknowledgements

The authors acknowledge financial support from Harbin Innovation Talents of Science and Technology Research Special Fund Project (Leader, 2012RFXXG005), Fundamental Research funds for the Central Universities, Natural Science Foundation of Heilongjiang Province (E201416), and Excellent Youth Foundation of Heilongjiang Province of China (JC201210).

Received: November 22, 2014
Revised: January 8, 2015
Published online: January 29, 2015

[1] P. Simon, Y. Gogotsi, *Nat. Mater.* **2008**, *7*, 845.
[2] Y. Zhao, J. Liu, Y. Hu, H. Cheng, C. Hu, C. Jiang, L. Jiang, A. Cao, L. Qu, *Adv. Mater.* **2013**, *25*, 591.
[3] Z. Fan, J. Yan, T. Wei, L. Zhi, G. Ning, T. Li, F. Wei, *Adv. Funct. Mater.* **2011**, *21*, 2366.
[4] X. Li, Q. Song, L. Hao, L. Zhi, *Small.* **2014**, *10*, 2122.
[5] H. Wang, H. S. Casalongue, Y. Liang, H. Dai, *J. Am. Chem. Soc.* **2010**, *132*, 7472.
[6] J. Yan, Q. Wang, T. Wei, Z. Fan, *Adv. Energy Mater.* **2014**, *4*, 1300816.
[7] Z. Chen, Y. Yuan, H. Zhou, X. Wang, Z. Gan, F. Wang, Y. Lu, *Adv. Mater.* **2014**, *26*, 339.
[8] L. H. Bao, J. Zhang, F. Li, *Nano Lett.* **2011**, *11*, 1215.
[9] S. Meher, G. Rao, *J. Phys. Chem. C.* **2011**, *115*, 15646.
[10] J. Yan, Z. Fan, T. Wei, W. Qian, M. Zhang, F. Wei, *Carbon* **2010**, *48*, 3825.
[11] J. Yan, Z. Fan, W. Sun, G. Ning, T Wei, Q. Zhang, R. Zhang, L. Zhi, F Wei, *Adv. Funct. Mater.* **2012**, *22*, 2632.
[12] L. Wang, Z. Dong, Z. Wang, F. Zhang, J. Jin, *Adv. Funct. Mater.* **2013**, *23*, 2758.
[13] H. Chen, L. Hu, Y. Yan, R. Che, M. Chen, L. Wu, *Adv. Energy Mater.* **2013**, *3*, 1636.
[14] M. Zhao, Q. Zhang, J. Huang, F. Wei, *Adv. Funct. Mater.* **2012**, *22*, 675.
[15] H. Chen, L. Hu, M. Chen, Y. Yan, L. Wu, *Adv. Funct. Mater.* **2014**, *24*, 934.
[16] L. Wang, D. Wang, X. Dong, Z. Zhang, X. Pei, X. Chen, B. Chen, J. Jin, *Chem. Commun.* **2011**, *47*, 3556.
[17] P. Vialat, C. Mousty, C. Taviot-Gueho, G. Renaudin, H Martinez, J. Dupin, E. Elkaim, F. Leroux, *Adv. Funct. Mater.* **2014**, *24*, 4831.
[18] M. Hu, X. Ji, L. Lei, X. Lu, *Electrochim. Acta* **2013**, *105*, 261.
[19] T. Yan, Z. J. Li, R. Y. Li, Q. Ning, H. Kong, Y. L. Niu, J. K. Liu, *J. Mater. Chem.* **2012**, *22*, 23587.
[20] J. Xu, S. Gai, F. He, N. Niu, P. Gao, Y. Chen, P. Yang, *J. Mater. Chem. A* **2014**, *2*, 1022.
[21] R. Ma, X. Liu, J. Liang, Y. Bando, T. Sasaki, *Adv. Mater.* **2014**, *26*, 4173.
[22] Z. Liu, R. Ma, M. Osada, K. Takada, T. Sasaki, *J. Am. Chem. Soc.* **2006**, *128*, 4872.
[23] X. Dong, L. Wang, D. Wang, C. Li, J. Jin, *Langmuir* **2012**, *28*, 293.
[24] H. Wang, H. Dai, *Chem. Soc. Rev.* **2012**, *10*, 1039.
[25] Z. Lu, W. Zhu, X. Lei, G. R. Williams, D. O'Hare, Z. Chang, X. Sun, X. Duan, *Nanoscale* **2012**, *4*, 3640.
[26] J. Cheng, J. H. Fang, M. Li, W. Zhang, F. Liu, X. Zhang, *Electrochim. Acta* **2013**, *114*, 68.
[27] Z. P. Liu, R. Z. Ma, M. Osada, N. Iyi, Y. Ebina, K. Takada, T. Sasaki, *J. Am. Chem. Soc.* **2006**, *128*, 4872.
[28] X. Wang, C. Yan, A. Sumboja, J. Yan, P. S. Lee, *Adv. Energy Mater.* **2013**, *4*, 1301240.
[29] J. Fang, M. Li, Q. Li, W. Zhang, Q. Shou, F. Liu, X. Zhang, J. Cheng, *Electrochim. Acta* **2012**, *85*, 248.
[30] J. Chen, C. Hsu, C. Hu, *J. Power Sources* **2014**, *253*, 205.
[31] R. Salunkhe, B. Bastakoti, C. Hsu, N. Suzuki, J. Kim, S. Dou, C. Hu, Y. Yamauchi, *Chem. Eur. J.* **2014**, *20*, 3084.
[32] C. Yu, J. Yang, C. Zhao, X. Fan, G. Wang, J. Qiu, *Nanoscale* **2014**, *6*, 3097.
[33] L. Zhang, X. Zhang, L. Shen, B. Gao, L. Hao, X. Lu, F. Zhang, B. Ding, C. Yuan, *J. Power Sources* **2012**, *199*, 395.
[34] Y. Hou, Y. W. Cheng, T. Hobson, J. Liu, *Nano Lett.* **2010**, *10*, 2727.
[35] J. Yan, Q. Wang, C. Lin, T Wei, Z. Fan, *Adv. Energy Mater.* **2014**, *4*, 1400500.
[36] R. Wang, X. Yan, J. Lang, Z. Zheng, P. Zhang, *J. Mater. Chem. A.* **2014**, *10*, 1039.
[37] H. Inoue, Y. Namba, E. Higuchi, *J. Power Sources* **2010**, *195*, 6239.
[38] Z. Wu, W. Ren, D. Wang, F. Li, Bi. Liu, H. Chen, *ACS Nano* **2010**, *4*, 5835.
[39] J. Chang, M. Jin, F. Yao, T. Kim, V. Le, H. Yue, F. Gunes, B. Li, A. Ghosh, S. Xie, Y. Lee, *Adv. Funct. Mater.* **2013**, *23*, 5074.
[40] Z. Chen, Y. Qin, D. Weng, Q. Xiao, Y. Peng, X. Wang, H. Li, F. Wei, Y. Lu, *Adv. Funct. Mater.* **2009**,*19*, 3420.
[41] M. Huang, Y. Zhang, F. Li, L. Zhang, Z. Wen, Q. Liu, *J. Power Sources* **2014**, *252*, 98.
[42] Q. Qu, Y. Shi, S. Tian, Y. H. Chen, Y. P. Wu, R. Holze, *J. Power Sources* **2009**, *194*, 1222.
[43] W. Jin, G. Cao, J. Sun, *J. Power Sources* **2008**, *175*, 686.
[44] Q. Qu, Y. Shi, L. Li, W. Guo, Y. Wu, H. Zhang, S. Guan, R. Holze, *Electrochem. Commun.* **2009**, *11*, 1325.
[45] J. W. Lang, L. B. Kong, M. Liu, Y. C. Luo, L. Kang, *J. Solid State Electr.* **2010**, *14*,1533.
[46] Y. Zhao, Y. Y. Wang, Q. Y. Lai, L. M. Chen, Y. J. Hao, X. Y. Ji, *Synthetic. Met.* **2009**, *159*, 331.
[47] J. Yan, Z. Fan, T. Wei, W. Qian, M. Zhang, F. Wei, *Carbon* **2010**, *48*, 3825.
[48] D. Pech, M. Brunet, H. Durou, P. H. Huang, V. Mochalin, Y. Gogotsi, P. L. Taberna, P. Simon, *Nat. Nanotechnol.* **2010**, *5*, 651.